

Article

Design, Synthesis and Antimicrobial Potential of Conjugated Metallopeptides Targeting DNA

Maria Camila Moreno-Ramirez ¹, Adriana Stefania Arias-Bravo ¹, Alberto Aragón-Muriel ^{1,2},
César Alonso Godoy ³, Yamil Liscano ⁴, Jose Oñate Garzón ^{5,*} and Dorian Polo-Cerón ^{1,*}

- ¹ Laboratorio de Investigación en Catálisis y Procesos (LICAP), Departamento de Química, Facultad de Ciencias Naturales y Exactas, Universidad del Valle, Cali 760001, Colombia; camimoreno610@gmail.com (M.C.M.-R.); adriana.stefania.arias@correounivalle.edu.co (A.S.A.-B.); aaragonm@unimagdalena.edu.co (A.A.-M.)
- ² Grupo de Investigaciones Bioquímicas (GIB), Universidad del Magdalena, Santa Marta 470004, Colombia
- ³ Laboratorio de Investigación en Biocatálisis y Biotransformaciones (LIBB), Grupo de Investigación en Ingeniería de los Procesos Agroalimentarios y Biotecnológicos (GIPAB), Departamento de Química, Facultad de Ciencias Naturales y Exactas, Universidad del Valle, Cali 760001, Colombia; cesar.godoy@correounivalle.edu.co
- ⁴ Grupo de Investigación en Salud Integral (GISI), Departamento Facultad de Salud, Universidad Santiago de Cali, Cali 760035, Colombia; yamil.liscano00@usc.edu.co
- ⁵ Grupo de Investigación en Química y Biotecnología (QUIBIO), Facultad de Ciencias Básicas, Universidad Santiago de Cali, Cali 760035, Colombia
- * Correspondence: jose.onate00@usc.edu.co (J.O.G.); dorian.polo@correounivalle.edu.co (D.P.-C.)

Abstract: Antimicrobial resistance threatens the effective prevention and treatment of an increasingly broad spectrum of infections caused by pathogenic microorganisms. This pressing challenge has intensified the search for alternative antibiotics with new pharmacological properties. Due to the chemical synergy between the biological activity of antimicrobial peptides (AMPs) and the different modes of action, catalytic properties, and redox chemistry of metal complexes, metallopeptides have emerged in recent years as an alternative to conventional antibiotics. In the present investigation, peptide ligands conjugated with 5-carboxy-1,10-phenanthroline (Phen) were prepared by solid-phase peptide synthesis (SPPS), and the corresponding copper(II) metallopeptides, Cu-PhenKG and Cu-PhenRG (where K = lysine, R = arginine, and G = glycine), were synthesized and characterized. The antimicrobial activities of these compounds toward Gram-positive and Gram-negative bacteria, evaluated by the broth microdilution technique, indicate that the metal center in the metallopeptides increases the antimicrobial activity of the complexes against the conjugated peptide ligands. Minimum inhibitory concentration (MIC) values of 0.5 µg/mL for *S. aureus* with the Cu-PhenKG complex and 0.63 µg/mL for *S. typhimurium* with the Cu-PhenRG complex were obtained. The MIC values found for the conjugated peptides in all microorganisms tested were greater than 1.5 µg/mL. The interactions of the conjugated peptides and their metallopeptides with plasmid DNA were evaluated by agarose gel electrophoresis. Alterations on the replication machinery were also studied by polymerase chain reaction (PCR). The results indicate that the complexes interact efficiently with pBR322 DNA from *E. coli*, delaying the band shift. Furthermore, the resulting DNA–metallopeptide complex is not a useful template DNA because it inhibits PCR, since no PCR product was detected. Finally, molecular dynamics and molecular docking simulations were performed to better understand the interactions of the obtained compounds with DNA. The Cu-PhenRG complex shows a significantly higher number of polar interactions with DNA, suggesting a higher binding affinity with the biopolymer.

Keywords: metallopeptide; antibacterial; metal complexes; biological activity; DNA interaction



Citation: Moreno-Ramirez, M.C.; Arias-Bravo, A.S.; Aragón-Muriel, A.; Godoy, C.A.; Liscano, Y.; Garzón, J.O.; Polo-Cerón, D. Design, Synthesis and Antimicrobial Potential of Conjugated Metallopeptides Targeting DNA. *Sci. Pharm.* **2024**, *92*, 21. <https://doi.org/10.3390/scipharm92020021>

Academic Editor: Claudio J. Salomón

Received: 7 February 2024

Revised: 2 April 2024

Accepted: 10 April 2024

Published: 17 April 2024



Copyright: © 2024 by the authors. Licensee MDPI, Basel, Switzerland. This article is an open access article distributed under the terms and conditions of the Creative Commons Attribution (CC BY) license (<https://creativecommons.org/licenses/by/4.0/>).

1. Introduction

In the last twenty years, global antimicrobial resistance has increased significantly, to the point that the World Health Organization (WHO) considers this phenomenon a public

health problem [1]. According to the WHO, the COVID-19 pandemic has led to an increase in the use of non-prescribed antibiotics, and therefore, an increase in antimicrobial resistance rates is expected after the pandemic, which will affect morbidity and mortality rates. The WHO also reported that 700,000 people die each year from drug-resistant infections, and if the current rate is maintained, it is estimated that this figure could increase to ten million by 2050, with a cost of more than USD 3 billion per year [2].

Currently, resistance to antibiotics is among the phenomena posing the greatest risks to human health. Every day, new and varied resistance mechanisms emerge and spread, posing a threat to people's capacity to effectively address common infectious diseases. As antimicrobials lose efficacy, infections such as pneumonia, tuberculosis, septicemia, and gonorrhoea are becoming increasingly difficult, and sometimes impossible, to treat [3]. Despite great efforts, the number of people affected is still too high, so it is necessary to develop new alternatives to this problem to protect human health. Antimicrobial peptides (AMPs) act as a natural defense mechanism against pathogens and invaders, and are produced by both prokaryotes and eukaryotes, representing an appealing antimicrobial model due to their broad spectrum of activity, a low likelihood for bacteria to develop resistance compared to conventional antibiotics, and extensive synergy with commonly used antimicrobials [4]. AMPs target mainly bacterial membranes. However, it has been reported that at a low MIC, such as 2 µg/mL, some AMPs can kill bacteria without altering the integrity of the membrane [5]. Instead of directly interacting with the membrane, AMPs with basic residues kill bacteria by having greater affinity for intracellular targets such as DNA phosphate groups [6]. The ability to translocate across the cell membrane depends on the presence of cationic residues such as arginine [7].

Antimicrobial macromolecules that contain metal ions have been shown to be effective against multiple microorganisms. The development of prodrugs whose active principles are organic ligands bound to transition metals has increased [8]. This interest is inspired, for example, by the known anticancer properties of cisplatin and its derivatives, or ferroquine, which is currently in clinical trials [9].

Metallopeptides combine the DNA-binding properties of metal complexes through electrostatic interactions, van der Waals interactions and/or covalent bonding with the specific binding possibilities offered by peptides through specific contact between the side chains of the peptide backbone and base pairs of DNA. The conformation of the peptide has a substantial impact on the coordination equilibria in the metal–peptide system, from both a thermodynamic and a structural perspective [10]. Aliphatic or aromatic chains form a spatial shield that prevents the hydrolysis of *N*-metal bonds and increases the structural strength of the complex molecule [11].

The inhibition of DNA synthesis is an important and widely used therapeutic strategy to treat hyperproliferative diseases such as bacterial infections, autoimmune disorders, and cancer. There are therapeutic agents used to inhibit DNA synthesis such as the cisplatin complex and its derivatives, which modify the composition and structure of nucleic acid [12]. Studies with modified copper and zinc tripeptides derived from M(II)-GlyGlyHis have reported various applications in the field of nucleic acid recognition and the design of selective cleavage agents, due to the unique structures of these metallopeptides and the contribution of the metal center [13]. Derivatives of phenanthroline and its metal complexes have been used as DNA intercalating agents due to their chemical characteristics, such as planarity, rigidity and hydrophobicity. For example, metal complexes incorporating 1,10-phenanthroline and other ligands were effective against multidrug-resistant strains of *Pseudomonas aeruginosa*, *Salmonella typhi*, *Staphylococcus aureus* and *Salmonella paratyphi*, or against fungi such as *Candida albicans* and *Cryptococcus neoformans* [14].

Therefore, considering the potential therapeutic uses of AMPs [15], in this study, we designed and synthesized metallopeptides incorporating AMPs along with their metal complexes, including Cu(II) and phenanthroline complexes, aiming to identify novel compounds with antimicrobial properties. The biological activity of these compounds was then evaluated against six pathogenic bacteria. Additionally, the interactions between

DNA–peptide and DNA–metallopeptide were analyzed, along with an examination of the impact of the compounds on PCR, in order to ascertain their functionality and efficacy against pathogenic bacteria.

2. Materials and Methods

2.1. Synthesis and Characterization

SPPS for short peptides was performed with the synthetic strategy Fmoc-tBu described by Meienhofer et al. [16]. Two compounds were synthesized, each consisting of two amino acids. The protected amino acids Fmoc-Gly-OH (99.0%, Novabiochem, Darmstadt, Germany), Fmoc-Arg(Pbf)-OH and Fmoc-Lys(Boc)-OH (98.0%, Sigma-Aldrich, St. Louis, MO, USA), and a derivative of phenanthroline, 5-carboxy-1,10-phenanthroline (Phen, Sigma-Aldrich), were used to form the conjugated peptide sequences presented in Figure 1 (Supplementary Materials Figure S2).

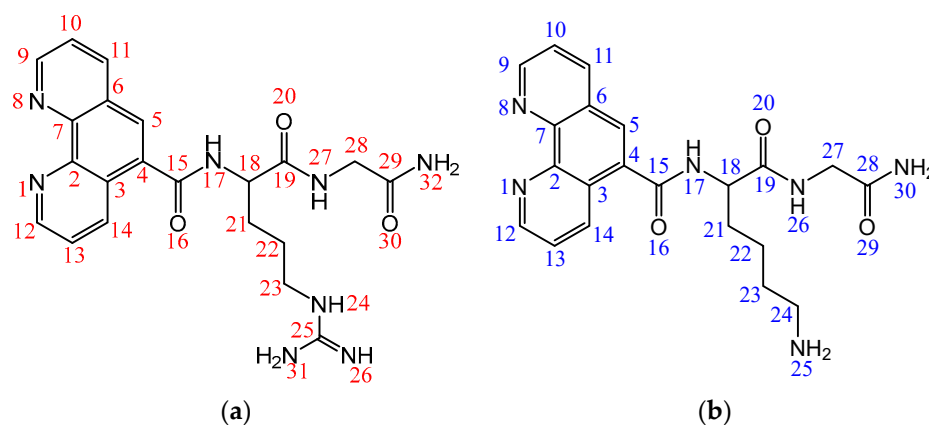


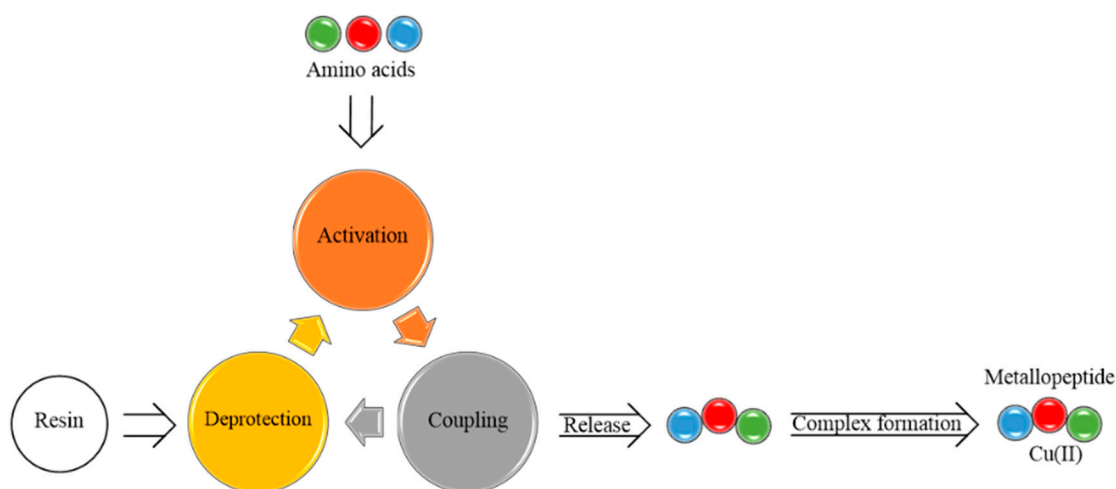
Figure 1. (a) Structure of 5-carboxy-1,10-phenanthroline, arginine, glycine (PhenRG). (b) Structure of 5-carboxy-1,10-phenanthroline, lysine, glycine (PhenKG).

PhenRG. ^1H NMR (400 MHz, D_2O): δ 1.76–1.82 (m, 2 H, $1 \times \text{CH}_2(22)\text{-Arg}$), δ 1.82–2.01 (m, 2 H, $1 \times \text{CH}_2(21)\text{-Arg}$), δ 3.24–3.27 (m, 2 H, $1 \times \text{CH}_2(23)\text{-Arg}$), δ 3.96–4.07 (m, 2 H, $1 \times \text{CH}_2(28)\text{-Gly}$), δ 4.62 (t, $J = \text{Hz}$ 1 H, $1 \times \text{CH}(18)\text{-Arg}$), δ 7.79–7.82 (q, $J = 4.0$ Hz, 2 H, $2 \times \text{CH}(10,13)\text{-Fen}$), δ 8.01 (s, 1 H, $1 \times \text{CH}(5)\text{-Phen}$), δ 8.45–8.47 (d, $J = 8.0$ Hz, 1 H, $1 \times \text{CH}(11)\text{-Phen}$), δ 8.60–8.62 (d, $J = 8.0$ Hz, 1 H, $1 \times \text{CH}(14)\text{-Phen}$), δ 8.91–8.92 (d, $J = 4.0$ Hz, 2 H, $2 \times \text{CH}(9,12)\text{-Phen}$). MS (FAB+): PhenRG ($\text{C}_{21}\text{H}_{24}\text{N}_8\text{O}_3$, MW: 436.48, m/z : 437), $[(\text{C}_{21}\text{H}_{24}\text{N}_8\text{O}_3\text{-H}_2\text{N}(\text{CNCNH})]$, MW: 408.46, m/z : 409), Phen- NH_2 $[(\text{C}_{21}\text{H}_{24}\text{N}_8\text{O}_3\text{-RGNH}_2 + \text{NH}_2)]$, MW: 223.24, m/z : 224). EA % (Calc.): %H = 5.49 (5.54), %C = 57.84 (57.79), %N = 26.63 (25.67).

PhenKG. ^1H NMR (400 MHz, D_2O): δ 1.62–1.68 (m, 2 H, $1 \times \text{CH}_2(22)\text{-Lys}$), δ 1.79–1.85 (m, 2 H, $1 \times \text{CH}_2(23)\text{-Lys}$), δ 1.99–2.08 (m, 2 H, $1 \times \text{CH}_2(21)\text{-Lys}$), δ 3.10 (t, $J = 8.0$ Hz, 2 H, $1 \times \text{CH}_2(24)\text{-Lys}$), δ 4.14–4.02 (m, 2 H, $1 \times \text{CH}_2(27)\text{-Gly}$), δ 4.67 (t, $J = 8.0$ Hz, 1 H, $1 \times \text{CH}(18)\text{-Lys}$), δ 7.87–7.90 (q, $J = 4.0$ Hz, 2 H, $2 \times \text{CH}(10,13)\text{-Phen}$), δ 8.08 (s, 1 H, $1 \times \text{CH}(5)\text{-Phen}$), δ 8.53–8.55 (d, $J = 8.0$ Hz, 1 H, $1 \times \text{CH}(11)\text{-Phen}$), δ 8.67–8.69 (d, $J = 8.0$ Hz, 1 H, $1 \times \text{CH}(14)\text{-Phen}$), δ 8.98–8.99 (d, $J = 4.0$ Hz, 2 H, $2 \times \text{CH}(9,12)\text{-Phen}$). MS (FAB+): PhenKG ($\text{C}_{21}\text{H}_{24}\text{N}_6\text{O}_3$, MW: 408.46, m/z : 410), $[(\text{C}_{21}\text{H}_{24}\text{N}_6\text{O}_3\text{-(CH}_2)_3\text{NH}_2\text{-2O-H-NH}_2)]$, MW: 306.15, m/z : 307), Phen- NH_2 $[(\text{C}_{21}\text{H}_{24}\text{N}_6\text{O}_3\text{-RGNH}_2 + \text{NH}_2)]$, MW: 223.24, m/z : 224). EA % (Calc.): %H = 5.88 (5.92), %C = 61.63 (61.75), %N = 20.66 (20.58).

The metallopeptides were obtained according to Scheme 1. The resin NovaPEG Rink Amide (35–100 mesh, 0.42 mmol/g, Sigma-Aldrich, St. Louis, MO, USA) was used for PhenRG [17], and Rink Amida (100–200 mesh, 0.55 mmol/g, Sigma-Aldrich) was used for PhenKG; the resins were previously swollen with *N,N*-dimethylformamide (DMF) to bind the first amino acid of each of the conjugated peptides. For activation of the carbonyl group, the reagent 2-(1H-Benzotriazole-1-yl)-1,1,3,3-tetramethylaminium tetrafluoroborate (TBTU) (99%, Alfa Aesar, Ward Hill, MA, USA) was used in combination with *N,N*-diisopropylethylamine (DIEA) (99.5%, Sigma-Aldrich) [18]. For deprotection of the amino group, piperazine was added

at concentrations of 10–20% in DMF/ethanol (9:1) [16,18,19]. Washing with DMF [19], isopropanol (IPA) and dichloromethane (DCM) was performed during coupling and deprotection.



Scheme 1. Synopsis of the reaction process for SPPS and complex formation.

To monitor the coupling and deprotection reactions of the amino groups of amino acids, a qualitative test for the detection of primary amines (Kaiser test) [20] and a test for SPPS using bromophenol blue as an indicator of free amino groups were carried out. Subsequently, the peptide was released from the resin with preliminary cleavages at 60–200 °C to determine the optimal time for the cleavage of the peptides. Once this value was obtained, the final cleavage was carried out using a “cleavage cocktail” containing phenol, TFA (99%, ReagentPlus, St. Louis, MO, USA) and radical scavengers such as triisopropylsilane (98%, Alfa Aesar), thioanisole (99%, ReagentPlus) and 1,2-ethanedithiol (98%, Sigma-Aldrich, St. Louis, MO, USA). Free peptide was precipitated using cold ethyl ether and collected by decantation after continuous centrifugation at 3000 rpm in a Clay Adams™ Compact II centrifuge [21]. The compounds were purified by dissolution in water and recrystallization from methanol. Analytical thin layer chromatography (TLC) was developed on TLC silica gel 60 F₂₅₄ plates under a 254 nm UV source. The conjugated peptides were pure according to the TLC criteria, and were therefore used in the next step without purification.

Complexation with the ligand was carried out using copper chloride CuCl₂ (97%, Sigma Aldrich, St. Louis, MO, USA) dissolved in water, which was mixed with the peptides synthesized above with a metal–ligand ratio of 2:1 solubilized in a water/methanol (7:3) mixture and allowed to react under constant stirring and at room temperature for five hours [8]. The resulting solution was crystallized by evaporation of the solvent until the complexes were obtained.

Cu-PhenRG. MS (FAB+): Cu-PhenRG (C₂₁H₂₄Cl₂CuN₈O₃, MW: 570.92): (C₂₁H₂₄ClCuN₈O₃, *m/z*: 534), (C₂₁H₂₄CuN₈O₃, *m/z*: 499), (C₂₀H₂₂CuN₆O₃, *m/z*: 460), (C₁₈H₁₈N₄O, *m/z*: 307). EA %(Calc.): %H = 4.30 (4.24), %C = 43.97 (44.18), %N = 19.27 (19.63).

Cu-PhenKG. MS (FAB+): Cu-PhenKG (C₂₁H₂₄Cl₂CuN₆O₃, MW: 542.91): (C₂₁H₂₄ClCuN₆O₃, *m/z*: 506), (C₂₁H₂₄CuN₆O₃, *m/z*: 471), (C₂₁H₂₄N₆O₃, PhenKG, *m/z*: 409). EA %(Calc.): %H = 4.51 (4.46), %C = 46.37 (46.46), %N = 15.63 (15.48).

For the characterization of the compounds, ¹H-NMR spectra were taken at 25 °C using deuterated water (D₂O) as a solvent in a Bruker Avance II 400 spectrometer. Elemental (C, H and N) analyses were carried out on a Flash EA 1112 Series CHN Analyzer (Thermo Fisher Scientific, Waltham, MA, USA). MS-FAB experiments were carried out on the compounds to find out their molecular weights. The results were recorded with a JEOL SX 102A mass spectrometer (JEOL, Peabody, MA, USA). ATR-Fourier transform infrared (FTIR) vibrational spectroscopy was used to elucidate the functional groups according to the main vibrational modes of the ligands and their complexes [8]. The collection of infrared spectra was performed within the wavenumber range of 4000 cm⁻¹ to 600 cm⁻¹ utilizing a

Shimadzu Affinity 1 device (FT-IR) equipped with an attenuated total reflectance (ATR) accessory (Shimadzu, Columbia, SC, USA).

2.2. Assessment of Biological Activity and Interactions with Biomolecules

The MIC was determined by the broth microdilution method according to protocols for antimicrobial susceptibility tests [22,23]. The conjugated peptides PhenRG and PhenKG and their corresponding complexes were analyzed against six bacteria, *Staphylococcus aureus* ATCC 25923, *Bacillus cereus* ATCC 10876, *Listeria monocytogenes* ATCC 19115, *Pseudomonas aeruginosa* ATCC 27853, *Salmonella typhimurium* ATCC 14028 and *Escherichia coli* ATCC 25922, with final inoculums of 5×10^6 CFU/mL and incubation at 37 °C for 18–24 h. The microplates (Ness Biotech Co., Ocala, FL, USA) included serial dilutions of the compounds in the range of 0.002–2 ($\mu\text{g/mL}$). In addition, a positive control (C+) and negative control (C–) were added to each microplate, with C+ consisting of Mueller–Hinton broth (MHB) with tetracyclin and C– containing only MHB. Ciprofloxacin (Cip) and Vancomycin were used as reference standards. All tests were performed in duplicate.

Interactions of Peptides and Metalloconjugates with Bacterial DNA

The interactions of the conjugated peptides and their metal complexes with bacterial DNA were evaluated by molecular biology assays using electrophoresis with 1% (*p/v*) agarose gel (Fisher BioReagents, Thermo Fisher Scientific, Waltham, MA, USA), $1 \times$ TAE buffer (pH 7.5) and 1 kb DirectLoad™ as molecular weight markers [24]. The Owl™ EasyCast™ B1 mini gel electrophoresis system and a power supply (C.B.S. Scientific EPS-300×, C.B.S. Scientific, San Diego, CA, USA) providing 100 V and 500 mA were used. The low- and medium-molecular-weight polymers polyethyleneimine (PEI), sodium dodecyl sulfate (SDS) and cetyl trimethylammonium bromide (CTAB) were used as reference standards in a 1:1 ratio with pBR322 plasmid DNA from *E. coli* (Sigma Aldrich). Each of the samples was incubated at 37 °C for 30 min using the Eppendorf ThermoMixer® C system. The gels were developed with GelGreen™ at a $1.2 \times$ concentration with a MaestroGen UltraBright® transilluminator (MaestroGen Inc., Hsinchu, Taiwan).

The effects of peptides and their complexes on the DNA synthesis process were analyzed by PCR [25]. For PCR, the following gender-specific primers targeting the Y chromosome (Y-DNA) that amplify the Q-M3 (Q1b1a1a) haplogroup with a C > T mutation were selected: 5'-AGGGCATCTTTCATTTTAGG-3' and 3'-GTGGATTGCTTTGTAGTAGG-5'. The analyzed samples were amplified in a volume of 15 μL with the addition of 0.32 μM primer M3, 0.1 mM dNTP mix (10 mM, Novagen®, Burlington, NJ, USA), 0.05 U/ μL DNA polymerase (5 U/ μL genTaq® Taq polymerase; Laboratorio de Genética y Biología Molecular LTDA), 5 mM MgCl_2 , $5 \times$ buffer and 50 ng Y-DNA. The individual PCR amplicon (300 pb) was performed using 8% polyacrylamide gel in $1 \times$ Tris, borate and EDTA (TBE) buffer in a 50 V electrophoretic run for 10 min followed by a run at 120 V for 30 min.

The PCRs were carried out in a Veriti™ thermal cycler. The amplification program began with a 1 min warm-up at 96 °C for initial denaturation, followed by 35 successive cycles of denaturation for 30 s at 94 °C, hybridization at 68 °C for 1 min, and extension at 72 °C for 30 s.

The PCR tests and the collection of DNA samples were carried out in the Human Molecular Genetics Laboratory of the Universidad del Valle, following all the parameters of the institutional committee for the review of human ethics and genetic counseling of the Universidad del Valle.

2.3. Calculation of Molecular and Pharmacokinetic Parameters

In silico evaluation of the compounds was carried out on the Swiss Institute of Bioinformatics (SIB) [26] and Molinspiration Cheminformatics platforms to assess the compounds' physicochemical parameters of absorption, distribution, metabolism, and excretion (ADME), their similarity to drugs and their pharmacokinetics. 3D models of the PhenKG, PhenKG-Cu, PhenRG and PhenRG-Cu compounds were constructed using SMILE code

and Avogadro version 1.2 software (<https://avogadro.cc/>, accessed on 3 December 2023) to optimize the structures with the “steepest descent” algorithm and the universal force field (UFF) [27]. The positive control Mitoxantrone was downloaded in PDB format from PubChem and used as a DNA intercalator in the receptor interaction experiment, which was previously experimentally validated. The ligand structures and control were prepared with Autodock [28] using Gasteiger charges [29]. The receptor molecule was DNA, which was optimized and prepared with Kollman charges. The coordinates of the grid were obtained from each molecule in the PDBs of the receptors, and the grid box was confirmed with the CB-Dock online tool (<http://cao.labshare.cn/cb-dock/>, accessed on 10 December 2023) (docking blind) using the prepared ligands and DNA.

Molecular docking analysis was performed, and the structure with the lowest energy was selected from a total of 50 runs using Autodock. Discovery Studio Visualizer version 2021 Client software (<http://accelrys.com>, accessed on 15 December 2023) was used to analyze the ligand–receptor interactions. Molecular dynamics simulations were carried out with Gromacs version 2022, but before that, the system was built with CharmmGUI (<https://www.charmm-gui.org/>, accessed on 15 December 2023) [30]. A KCl concentration of 0.15 M was used, and the ions in the system were located by the Monte Carlo method with a water thickness of 22.5 Å using the CHARMM36m force field [31]. The systems were adjusted by slowly heating them to a temperature of 310 K for 75 ps. For equilibrium, 90,000,000 numsteps were used. Once the system was equilibrated to the desired temperature and pressure, the molecular dynamics simulations were performed for 20 ns, since the interactions between the DNA and the ligands lasted less than this time. PyMOL was used to extract the PDB molecules from the simulation and analyze the interactions with Discovery Studio every ns until 20 ns was reached.

3. Results and Discussion

3.1. Synthesis and Characterization

The IR spectra for each of the ligands show the main absorption bands of amides I, II and III in the regions of 1600–1700, 1500–1600, and 1200–1350 cm^{-1} , respectively [32]. The amide I band is produced by bending vibrations of the C=O bond of the peptide coupled to the stretching vibrations of the C–N bond, the amide II band comes from N–H bending and CN stretching vibrations, and the absorption of amide III is assigned to C–N stretching vibrations linked to bending vibrations in the N–H plane, with weak contributions from C–C and C=O stretching [33]. Bands associated with the N–H bending of primary and secondary amines and amides are in the range of 3180–3500 cm^{-1} , and bending vibrations for aromatics appear at 3100–3300 cm^{-1} (Figure S1).

NMR constitutes a useful analytical methodology for studying the structure, function and dynamics of molecules in solution, which is why this technique is used to characterize peptides. In the preliminary analysis, the most relevant signals were identified in the ^1H -NMR spectra according to the numbering in Figure 1. The proton NMR spectrum for the PhenRG peptide is presented in Figure S3. The signals at δ 7.76–9.01 ppm refer to the shifts of the seven hydrogens in phenanthroline. Where H11 and H14 appear as doublets, it is considered that one of these two protons is closer to the C=O group of phenanthroline, since the three-dimensional arrangement of Phen can displace one of these hydrogens to a high field due to the adjacent electron-attracting group [34]. In contrast, H9 and H12 are shown as a doublet (d, 2H). The signals at high field were assigned to the peptide chain and the arginine side chain. The signal for the methylene group (αH) of the glycine residue was assigned at δ 3.96–4.05 ppm (m, 2H) and numbered H28. Regarding the R residue, the signals at δ 4.62 ppm (t, 1H) and δ 1.93–1.95 ppm (m, 2H) correspond to the methine in H18 and the methylene H21, belonging to αH and βH of the residue. Similarly, the shifts at δ 4.79 ppm and δ 2.01 ppm are related to the peaks of the residual solvents of D_2O and acetic acid [35]. Similarly, in the spectrum corresponding to PhenKG (see Figure S4), the protons corresponding to the aromatic rings are observed; in the case of methine located in H5, its displacement appears at δ 8.07 ppm (s, 1H). The shifts at δ 4.67 ppm (t, 1H) and

δ 2.01–2.03 ppm (m, 2H) were attributed to methine and methylene, H18 and H21, from lysine (α H and β H). Furthermore, H22 and H24 are proposed to exhibit signals at 1.95–2.06 ppm (m, 2H) and 1.59–1.69 ppm (m, 2H), respectively. Finally, the signals at δ 4.05–4.10 ppm (d, 2H) were assigned to H27, methylene from glycine.

Proteomic analysis was performed by fast atom bombardment (FAB) ionization mass spectrometry [36]. Figures S5–S8 indicate that for the peptides and the metallopeptides, the molecular ions $[M + 1]$ coincide with the molecular weights. Likewise, a base peak at 154 m/z is observed for all compounds, including ligands and complexes. The results for these compounds confirm the presence of the peptide and complex.

3.2. Studies of Biological Activity and Interactions with Biomolecules

The biological activities of the obtained compounds were evaluated in three Gram-positive and three Gram-negative bacteria to determine the MIC, defined as the minimum concentration of an antimicrobial ($\mu\text{g}/\text{mL}$) that inhibits the visible growth of a microorganism after 18–24 h of incubation at 37 °C [37].

Table 1 shows that the PhenRG peptide and its metallopeptide are generally more effective against all bacterial strains tested than the PhenKG compound and its complex. It is inferred that the guanidinium group in Arg side chains forms bidentate interactions with the DNA phosphate groups.

Table 1. Antibacterial activity of the synthesized compounds.

| Compound | MIC ($\mu\text{g}/\text{mL}$) | | | | | |
|------------|---------------------------------|------------------|-------------------------|----------------------|-----------------------|----------------|
| | <i>S. aureus</i> | <i>B. cereus</i> | <i>L. monocytogenes</i> | <i>P. aeruginosa</i> | <i>S. typhimurium</i> | <i>E. coli</i> |
| | ATCC 25923 | ATCC 10876 | ATCC 19115 | ATCC 27853 | ATCC 14028 | ATCC 25922 |
| PhenKG | >2 | >2 | >2 | >2 | >2 | >2 |
| Cu-PhenKG | 0.5 | >2 | 2 | >2 | 2 | 2 |
| PhenRG | >1.25 | >1.25 | >1.25 | >1.25 | >1.25 | >1.25 |
| Cu-PhenRG | 1.25 | >1.25 | 1.25 | >1.25 | 0.63 | 1.25 |
| Cip | ≤ 0.5 | ≤ 0.5 | ≤ 0.5 | ≤ 0.5 | ≤ 0.5 | ≤ 0.5 |
| Vancomycin | ≤ 4 * | 3* | ≤ 2 * | - | - | - |

* Reference values not included in this research [38,39].

The incorporation of metal ions in each of the peptides resulted in an increase in antimicrobial activity (Table 1); the activity of Cu-PhenKG against *S. aureus* was 0.5 $\mu\text{g}/\text{mL}$, and an MIC of 0.63 $\mu\text{g}/\text{mL}$ against *S. typhimurium* was obtained for Cu-PhenRG. The MIC reduction could be associated with the interaction of the complex with DNA through insertion in the minor or major groove, which stabilized the adducts via hydrophobic effects between Phen and DNA, as well as C–H interactions involving the heteroatoms of the complex [40]. In addition, comparison of the MIC values against *S. aureus* of Cu-PhenKG and vancomycin, whose MIC is ≤ 4 $\mu\text{g}/\text{mL}$ [41], suggests that the results obtained in this study are promising, since the reference antibiotic is a glycopeptide used as the primary treatment option for Gram-positive bacteria at strains of methicillin-resistant *S. aureus* (MRSA). Ciprofloxacin was also used as a reference in the tests, with MIC ≤ 0.5 $\mu\text{g}/\text{mL}$. A comparison of this value with that obtained for Cu-PhenRG against *S. typhimurium* also suggests that the results are promising because, although Cip is more effective, it should be taken into account that the rate of resistance emergence against ciprofloxacin is higher than that generated by AMPs [42].

To determine the interactions of the conjugated peptides and their metallopeptides with DNA, the change in electrophoretic mobility of the protein–nucleic acid complex was evaluated. Differences in the properties of the protein–nucleic acid complex, such as changes in the conformation of DNA, make its migration slower than that of the corresponding free nucleic acid [43]. Variations in migration are also attributable to external factors, which include the composition of the gel matrix and the electrophoresis tempera-

ture [38]. PEI, SDS and CTAB were used as references in the interaction of the compounds with DNA [44].

In Figures 2 and 3, PEI formed a complex with the DNA showing null mobility, suggesting that the size of the PEI–DNA complex slows movement through the gel. Furthermore, its cationic property and the charge of PEI predominate, possibly covering the DNA through interactions between the phosphate groups of DNA and the amino groups of PEI. These interactions involve both electrostatic forces and hydrogen bonding [45], similar to the in vivo behavior of histones (cationic proteins) in chromatin of eukaryotic cells. In contrast, at the concentrations evaluated, SDS and CTAB did not generate a stable complex with DNA, thus leaving its mobility unchanged. This is possibly due to charge repulsion in the case of SDS and the formation of CTAB micelles that do not interact effectively with DNA.

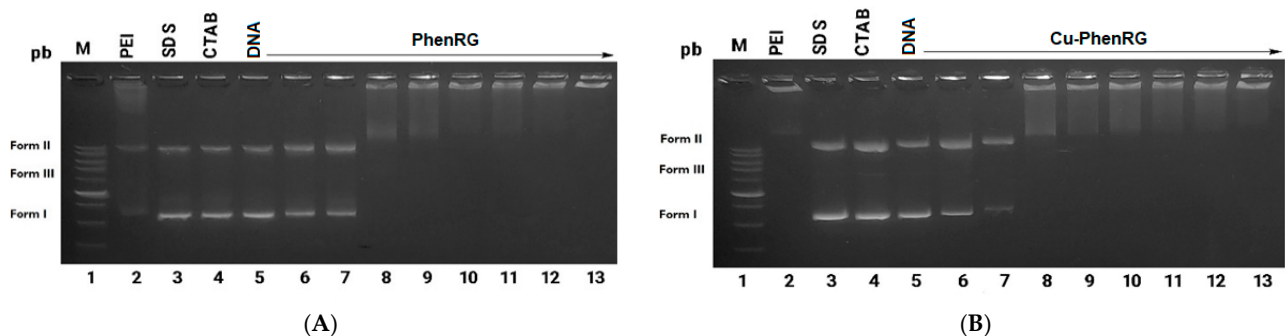


Figure 2. Agarose gel electrophoresis of *E. coli* pBR322 with the synthesized conjugated peptides and metalloptides. Lane 1: Molecular weight standard, M (1 kb). Lane 2: DNA/PEI (1:1). Lane 3: DNA/SDS (1:1). Lane 4: DNA/CTAB (1:1). Lane 5: plasmid DNA pBR322 (9 ng/μL). Lanes 6 to 13: DNA with increasing concentrations of the compound (0.125, 0.25, 0.5, 1.0, 1.5, 2.0, 2.5, 3.0 μM). (A) PhenRG; (B) Cu-PhenRG.

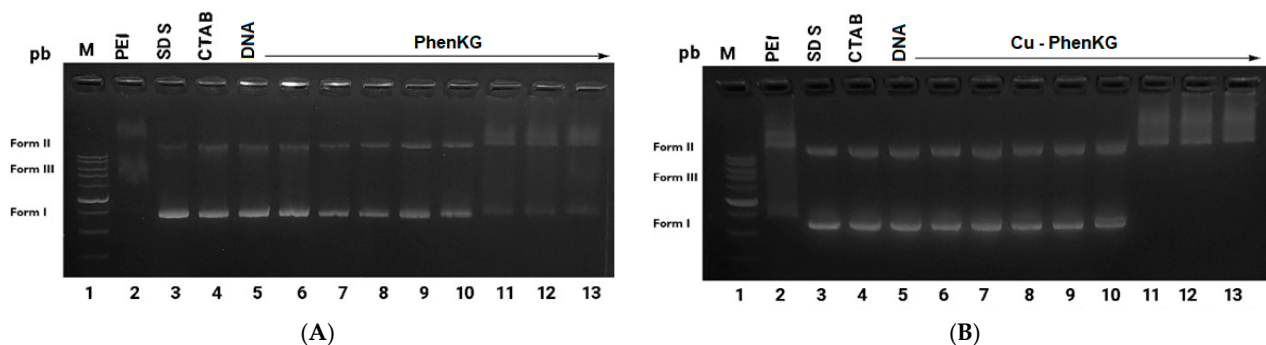


Figure 3. Agarose gel electrophoresis of *E. coli* pBR322 with the synthesized conjugated peptides and metalloptides. Lane 1: Molecular weight standard, M (1 kb). Lane 2: DNA/PEI (1:1). Lane 3: DNA/SDS (1:1). Lane 4: DNA/CTAB (1:1). Lane 5: plasmid DNA pBR322 (9 ng/μL). Lanes 6 to 13: DNA with increasing concentrations of the compound (0.125, 0.25, 0.5, 1.0, 1.5, 2.0, 2.5, 3.0 μM). (A) PhenKG; (B) Cu-PhenKG.

According to the results of the electrophoretic mobility shift assay (Figure 2), a two-phase interaction between plasmid DNA and the compounds PhenRG and Cu-PhenRG can be observed: at low compound concentrations (initial phase), it acts cleaving the phosphodiester bond, stabilizing form II (nicked circular) [46,47]. Thus, the DNA of form I decreases in quantity, and that in form II increases (Figure 2B, bands in lanes 6 and 7 compared to those of lane 5 or control DNA). Since III form is not detected, this indicates that the DNA may not have been permanently broken, or if it was, only single strand breaks occurred, maintaining circularity [46,47]. Then, in the second phase, compound

concentrations equal to or greater than $\sim 0.5 \mu\text{M}$ cause most of the DNA to acquire form II, and the interactions between plasmid DNA and conjugated peptides increase, resulting in complexes with a growing number of compound molecules. This is probably due to the fact that DNA form II, given its open structure, becomes more accessible to the conjugated peptides, favoring the formation of ionic, polar or even intercalation interactions with the aromatic moiety of the synthesized compounds. Hence, the generated complexes tend to have gradually less negative charge as more compound molecules are incorporated, thus losing their electrophoretic mobility until it becomes null, similarly to the effect caused by PEI.

The two-phase interaction behavior appears to manifest with PhenKG and its complex with Cu(II) as well (Figure 3). The distinctions lie in the fact that the transition between phases occurs at a higher concentration ($\sim 2 \mu\text{M}$), possibly due to the weaker H-bonding interaction of the lysine residue (monodentate) with the DNA phosphodiester groups compared to that of the arginine residue (bidentate) [48]. These results are consistent with the antibacterial activity (Table 1), for which it was described that the presence of Arg slightly increases the reactivity against *E. coli*. Additionally, for Cu-PhenKG, the metal appears to favor the stabilization of DNA complexes with lower mobility (see Figure 3A,B, lanes 11 to 13; notice that in 3b DNA disappear completely), unlike what happened with Cu-PhenRG, where the metal seems to contribute in this in a lower degree. Therefore, the results suggest that the metal contributes to increasing the interaction of the complex with DNA. Most of the transition metals react chemically with the N7 atom of purine or N3 of pyrimidine, and perturb the double helix, since they usually disrupt base pair–hydrogen bonding and destabilize the double helix [49].

PCR is a technique that exploits the natural catalytic properties of a DNA polymerase during DNA replication to amplify a specific DNA segment in vitro. Assessing the yield of a PCR reaction in the presence of test compounds can provide insights into their mechanisms as potential antimicrobial agents, such as inhibiting the in vivo DNA replication process [50].

PCR inhibitors may interfere with the DNA amplification process through DNA degradation processes, nucleic acid binding, interaction with Mg^{2+} ions, or by preventing binding with the DNA polymerase [51]. The activity of inhibitory substances in PCR can be studied by monitoring the presence or absence of PCR products at the end of thermal cycling using gel electrophoresis, high-pressure liquid chromatography or microtitering [52].

In this context, we evaluated the potential effects of the synthesized compounds in a standard PCR by examining their impacts under varying concentrations of PhenRG and PhenKG, along with their respective Cu complexes. Figures 4–7 show the polyacrylamide gel electrophoresis obtained for each of the tests with PCR products corresponding to a 300 bp amplicon. Noticeable PCR inhibition was observed from $\sim 2.5 \mu\text{M}$ for PhenKG and from $\sim 1.7 \mu\text{M}$ for Cu-PhenKG (Figures 4 and 5). For PhenRG and Cu-PhenRG, the values were from $\sim 1.7 \mu\text{M}$ and from $\sim 2.0 \mu\text{M}$, respectively (Figures 6 and 7). Again, the presence of the metal implies different effects, these being slightly positive (lower inhibition concentration) for the peptide containing K and slightly negative for that with R as PCR inhibitors. Similar to the electrophoretic mobility shift assay, we observe a two-phase behavior in the PCR inhibition, and see that the conjugated peptides containing R were more effective than their counterparts containing K. This suggests a potential causal link between the observed effects, namely, that the formation of specific DNA complexes above a critical initial concentration of conjugated peptides makes the DNA template nonfunctional by the polymerase. It has long been known that some compounds that interact with DNA can prevent the binding of DNA polymerase [50]. However, we cannot exclude the possibility of compounds also interfering with the function of the oligonucleotides used as primers, or with the polymerase itself.

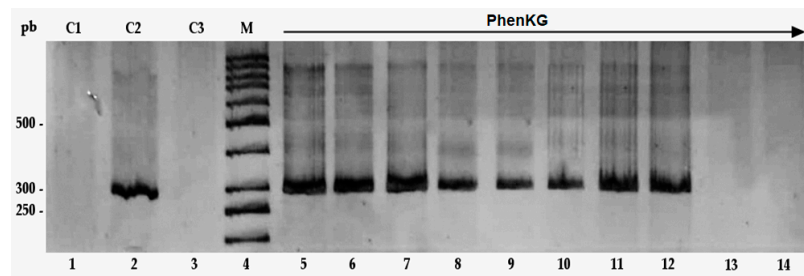


Figure 4. Results of 8% polyacrylamide gel electrophoresis. Lane 1: PCR negative control, C1. Lane 2: PCR positive control, C2. Lane 3: peptide negative control, C3. Lane 4: molecular weight marker, M (25 bp). Lanes 5 to 14: increasing concentrations of the PhenKG peptide (0.2, 0.5, 0.7, 1.0, 1.2, 1.5, 1.7, 2.0, 2.5, 3.0 μ M).

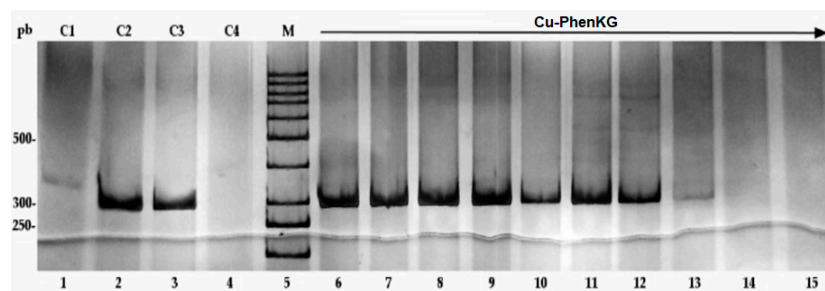


Figure 5. Results of 8% polyacrylamide gel electrophoresis. Lane 1: PCR negative control, C1. Lane 2: PCR positive control, C2. Lane 3: peptide negative control, C3. Lane 4: molecular weight marker, M (25 bp). Lanes 5 to 14: increasing concentrations of the Cu-PhenKG peptide (0.2, 0.5, 0.7, 1.0, 1.2, 1.5, 1.7, 2.0, 2.5, 3.0 μ M).

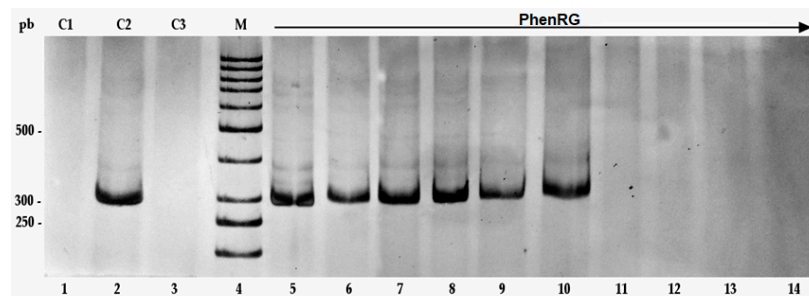


Figure 6. Results of 8% polyacrylamide gel electrophoresis. Lane 1: PCR negative control, C1. Lane 2: PCR positive control, C2. Lane 3: peptide negative control, C3. Lane 4: molecular weight marker, M (25 bp). Lanes 5 to 14: increasing concentrations of the PhenRG peptide (0.2, 0.5, 0.7, 1.0, 1.2, 1.5, 1.7, 2.0, 2.5, 3.0 μ M).

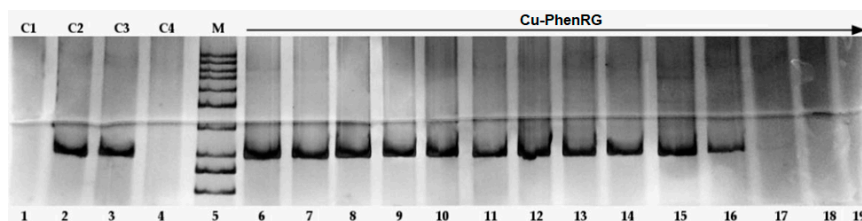


Figure 7. Results of 8% polyacrylamide gel electrophoresis. Lane 1: PCR negative control, C1. Lane 2: PCR positive control, C2. Lane 3: peptide negative control, C3. Lane 4: molecular weight marker, M (25 bp). Lanes 5 to 14: increasing concentrations of the Cu-PhenRG peptide (0.2, 0.5, 0.7, 1.0, 1.2, 1.5, 1.7, 2.0, 2.5, 3.0 μ M).

Finally, considering that PCR as a process analogous to DNA replication requires *in vivo* during cell division, it is suggested that the synthesized conjugated peptides and metalloptides could impact not only the cell membrane, but also cell reproduction.

Table 2 shows the different binding energies between the compounds studied and the receptor (DNA). Mitoxantrone is used as a control, which is a drug with anticancer activity, and which binds irreversibly to DNA. When the binding energy values are compared, it is observed that Cu-PhenKG and Cu-FhenRG have significantly stronger bonding energies compared to free ligands, so the presence of the metal has a determining effect on the bond to DNA. This is consistent with the results of electrophoretic mobility shift and PCR inhibition assays, especially for the peptide containing K. These data could be important for understanding the ability of different molecules to interact with DNA, which could have implications in a variety of fields, such as medicinal chemistry or gene therapy.

Table 2. Binding energies between compounds and the DNA receptor.

| Compound | Binding Energy (kJ/mol) |
|--------------|-------------------------|
| Mitoxantrone | −6.8 |
| PhenKG | −6.8 |
| Cu-PhenKG | −11.2 |
| PhenRG | −6.8 |
| Cu-PhenRG | −11.1 |

In Figure 8, the hotspots or points of greatest number of interactions of the PhenKG and Cu-PhenKG compounds with DNA can be analyzed. These hotspots correspond to the DNA residues with which the ligands have a greater affinity, and are related to their biological activity. In the case of Cu-PhenKG, it is observed that it establishes a complex interaction with DNA, forming eight hydrogen bonds, one halogen interaction, and two hydrophobic interactions. This diversity in interaction types suggests a multifaceted and robust binding mode, which could be the key behind its high negative binding energy, indicating a strong affinity for DNA.

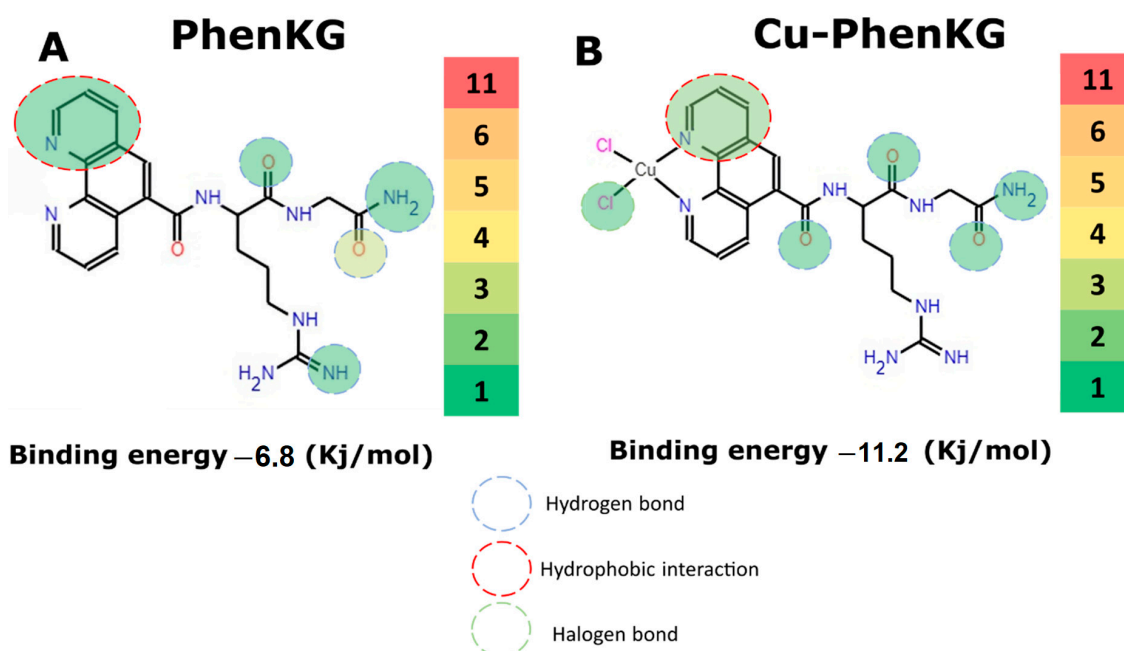


Figure 8. Interaction hotspots. Figure (A) presents the interaction hotspots for the PhenKG molecule, highlighting the hydrogen, hydrophobic, and halogen bonding sites. In the two-dimensional representation, hydrogen bonds are indicated by blue dashed lines, hydrophobic interactions by red dashed circles, and halogen bonds by green dashed circles. Figure (B) presents the interactions for the Cu-PhenKG

molecule. The color intensity of the circles ranges from green to red, corresponding to the number of interactions, with green representing a single interaction and red signifying up to eight interactions.

Cu-PhenRG, on the other hand, has a unique set of interactions, with four hydrogen bonds, two halogen interactions, and one hydrophobic interaction (Figure 9). While Cu-PhenKG has a greater number of hydrogen bonds than Cu-PhenRG, the presence of an extra-halogen interaction has a notable impact. The different molecular architecture of this compound may be an important reason for its strong attraction to DNA, illustrating how differences in the type and number of molecular interactions directly impact the compound's ability to bind DNA.

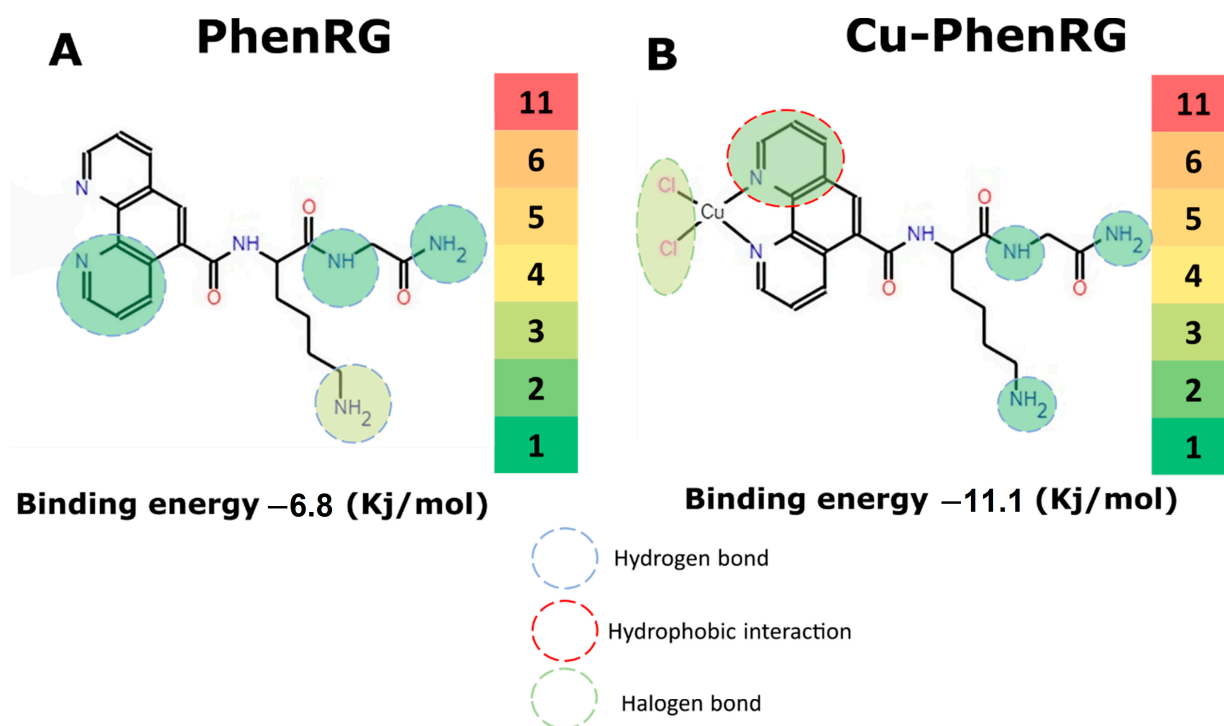


Figure 9. Interaction hotspots. Figure (A) presents the interaction hotspots for the PhenRG molecule, highlighting the hydrogen, hydrophobic, and halogen bonding sites. In the two-dimensional representation, hydrogen bonds are indicated by blue dashed lines, hydrophobic interactions by red dashed circles, and halogen bonds by green dashed circles. Figure (B) presents the interactions for the Cu-PhenRG molecule. The color intensity of the circles ranges from green to red, corresponding to the number of interactions, with green representing a single interaction and red signifying up to eight interactions.

3.3. Calculation of Molecular and Pharmacokinetic Parameters

Potential drug compounds possess adequate ADME properties and defined physico-chemical properties. The synthesized compounds were submitted to the SwissADME and Molinspiration Cheminformatics platforms to verify their properties. Table 3 shows the obtained molecular weight, number of rotating bonds, number of hydrogen bond acceptors (O and N atoms), number of hydrogen bond donors (groups OH y NH), solubility (Log S), topological polar surface area (TPSA), *n*-octanol/water partition coefficient (log $P_{o/w}$, MLOGP) and Lipinski filter. PhenRG has a low probability of being an oral drug since it violates two of the five Lipinski rules: one is related to the number of nitrogens or oxygens, and the second is related to the NH and OH groups in the structure, which influence the absorption and permeability potential in the intestinal epithelium [26].

Table 3. Molecular and physicochemical properties.

| Compound | Molecular Weight (g/mol) | Rotary Bonds | H-Acceptor Bonds | H-Donor Bonds | LogS (ESOL) | TPSA (Å ²) | Log P _{o/w} (MLOGP) | Lipinski Filter |
|----------|--------------------------|--------------|------------------|---------------|--------------|------------------------|------------------------------|---|
| PhenKG | 408.46 | 11 | 6 | 4 | Soluble | 153.09 | −0.41 | Yes; 0 violation |
| PhenRG | 436.47 | 12 | 6 | 6 | Very Soluble | 188.97 | −0.79 | No; 2 violations: N or O > 10, NH or OH > 5 |

Regarding the bioavailability radars, the following properties were considered, where the area in pink represents the optimal range for each property: XLOGP3 lipophilicity (−0.7, +5.0), molecular weight, polarity, solubility (log S) < 6, saturation (sp³ hybridizing carbons) > 0.25 and flexibility < 9 bonds with rotation. Thus, the radar graph of a compound must be completely within the pink area to be considered similar to a drug. As seen in Figure 10, the predictive models indicate that radars a and b show a pharmacokinetic behavior that is not totally suitable for the design of an oral drug, so the compounds are not bioavailable because they are polar and too flexible [26], especially PhenRG.

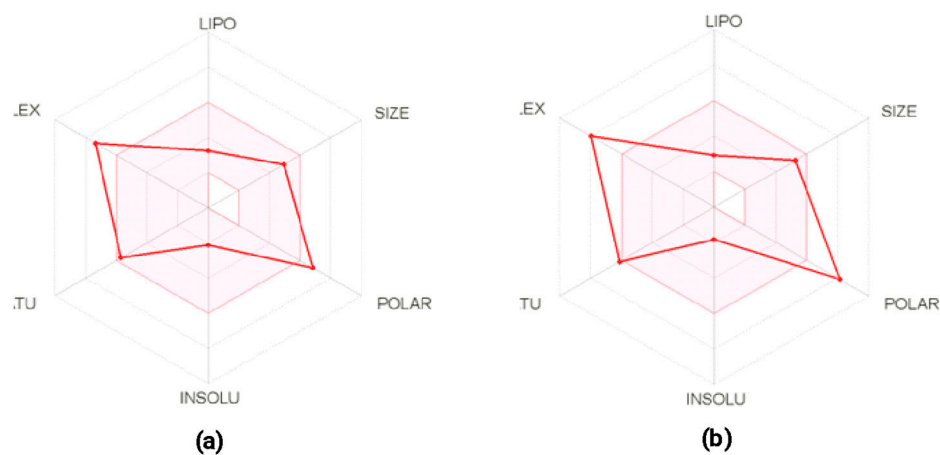


Figure 10. Bioavailability radars. (a) PhenKG and (b) PhenRG. Each axis of the radar represents a distinct property that affects the bioavailability of the molecules. “LIPO” reflects lipophilicity, important for absorption and cellular permeability. “SIZE” denotes molecular size, which is crucial for diffusion through biological barriers. “POLAR” measures polarity, influencing the molecule’s solubility and transport. “INSOLU” indicates insolubility, a critical aspect for drug formulation and oral administration. “TU” is understood as insaturation, which can affect chemical reactivity and molecular interactions. “EX” assesses molecular flexibility, which can impact how the molecule binds to its target and its overall bioactivity.

Regarding the pharmacokinetics described in Table 4, none of the peptides are well absorbed in the gastrointestinal tract (GI). Furthermore, PhenKG is a substrate for p-glycoprotein (P-gp), which affects its efficacy as a drug. The interaction with cytochrome P450 is important for the elimination of drugs through metabolic biotransformation, which suggests that the inhibition of these isoenzymes is one of the main causes of pharmacokinetic interactions with toxic and other unwanted effects due to the lower clearance and the accumulation of the drug. No evidence of inhibition was observed for any of the five main isoforms CYP1A2 (cytochrome P450 1A2), CYP2C19 (cytochrome P450 2C19), CYP2C9 (cytochrome P450 2C9), CYP2D6 (cytochrome P450 2D6), and CYP4A4 (c 3), thus reducing possible drug interactions.

In summary, the chemoinformatic analysis of the synthesized compounds indicates that the PhenRG peptide is less likely to be an oral drug than PhenKG because it violates two Lipinski rules. The accuracy of predictions based on the Lipinski rule is up to 73%, and 20% of the drugs approved to be used orally violate at least one of the parameters of rule 5 [53].

Table 4. Pharmacokinetics of the compounds.

| Compound | Absorption GI | Substrate P-gp | Inhibitor | | | | |
|----------|---------------|----------------|-----------|---------|--------|--------|--------|
| | | | CYP1A2 | CYP2C19 | CYP2C9 | CYP2D6 | CYP3A4 |
| PhenKG | Low | Yes | No | No | No | No | No |
| PhenRG | Low | No | No | No | No | No | No |

4. Conclusions

The synthesis and characterization of short conjugated peptides and metalloptides were carried out. The results of characterization techniques such as IR, NMR, and MS confirm the presence of the expected compounds. Molecular biology tests show that peptides and complexes that contain arginine present better results as potential antibacterial agents than do those that have a lysine residue, even achieving values of 1.26 μM (0.63 $\mu\text{g}/\text{mL}$), as in the case for *S. typhimurium* with Cu-PhenRG.

Regarding the interaction with DNA, a two-phase interaction mechanism is suggested; concentrations equal to or higher than 0.5 μM for PhenKG and Cu-PhenKG and 2 μM for PhenRG and Cu-PhenRG generated important alterations in DNA structure. Likewise, the PCR tests show that the compounds lowered the amplicon yield, suggesting the inhibition of DNA replication as a possible mechanism of inhibition of cell proliferation.

Finally, the outcomes of both the in vivo and in vitro experiments reveal a synergistic effect on the metalloptides, which aligns with the observations made in the in silico assessments, where the affinity energy between the metalloptides and DNA is found to be reduced. These findings could be important for understanding the abilities of different molecules to interact with DNA, which could have implications in a variety of fields, such as medicinal chemistry or gene therapy.

Supplementary Materials: The information can be downloaded at: <https://www.mdpi.com/article/10.3390/scipharm92020021/s1>.

Author Contributions: Conceptualization, J.O.G., C.A.G. and D.P.-C.; methodology, M.C.M.-R., A.S.A.-B., A.A.-M., C.A.G. and J.O.G.; software, Y.L.; validation, J.O.G., C.A.G. and D.P.-C.; formal analysis, J.O.G., C.A.G., Y.L. and D.P.-C.; investigation, M.C.M.-R., A.S.A.-B., A.A.-M. and C.A.G.; resources, J.O.G. and D.P.-C.; data curation, J.O.G., C.A.G., Y.L. and D.P.-C.; writing—original draft preparation, M.C.M.-R. and A.S.A.-B.; writing—review and editing, J.O.G., C.A.G., Y.L. and D.P.-C.; visualization, Y.L. and D.P.-C. supervision, J.O.G., C.A.G. and D.P.-C.; project administration, D.P.-C.; funding acquisition, J.O.G., C.A.G. and D.P.-C. All authors have read and agreed to the published version of the manuscript.

Funding: This research was funded by the Universidad del Valle (CI 71271) and Universidad Santiago de Cali under grant number DGI-COCEIN 934-621120-2388 and Dirección General de Investigaciones of Universidad Santiago de Cali under call No. 01-2024.

Institutional Review Board Statement: Not applicable.

Informed Consent Statement: Not applicable.

Data Availability Statement: Data are available in the manuscript.

Acknowledgments: The authors are grateful to Secretaría de Salud del Valle del Cauca—Complejo Integral de Servicios de Salud Pública Aníbal Patiño Rodríguez for providing the space and the bacterial strains for the antimicrobial assays.

Conflicts of Interest: The authors declare no conflicts of interest.

References

1. Rogers Van Katwyk, S.; Grimshaw, J.M.; Nkangu, M.; Nagi, R.; Mendelson, M.; Taljaard, M.; Hoffman, S.J. Government Policy Interventions to Reduce Human Antimicrobial Use: A Systematic Review and Evidence Map. *PLoS Med.* **2019**, *16*, e1002819. [[CrossRef](#)] [[PubMed](#)]
2. Juliano, S.A.; Serafim, L.F.; Duay, S.S.; Heredia Chavez, M.; Sharma, G.; Rooney, M.; Comert, F.; Pierce, S.; Radulescu, A.; Cotten, M.L.; et al. A Potent Host Defense Peptide Triggers DNA Damage and Is Active against Multidrug-Resistant Gram-Negative Pathogens. *ACS Infect. Dis.* **2020**, *6*, 1250–1263. [[CrossRef](#)] [[PubMed](#)]

3. Bergkessel, M.; Forte, B.; Gilbert, I.H. Small-Molecule Antibiotic Drug Development: Need and Challenges. *ACS Infect. Dis.* **2023**, *9*, 2062–2071. [[CrossRef](#)] [[PubMed](#)]
4. Valenti, G.E.; Alfei, S.; Caviglia, D.; Domenicotti, C.; Marengo, B. Antimicrobial Peptides and Cationic Nanoparticles: A Broad-Spectrum Weapon to Fight Multi-Drug Resistance Not Only in Bacteria. *Int. J. Mol. Sci.* **2022**, *23*, 6108. [[CrossRef](#)] [[PubMed](#)]
5. Patrzykat, A.; Friedrich, C.L.; Zhang, L.; Mendoza, V.; Hancock, R.E.W. Sublethal Concentrations of Pleurocidin-Derived Antimicrobial Peptides Inhibit Macromolecular Synthesis in *Escherichia coli*. *Antimicrob. Agents Chemother.* **2002**, *46*, 605–614. [[CrossRef](#)] [[PubMed](#)]
6. Rivera-Sánchez, S.P.; Agudelo-Góngora, H.A.; Oñate-Garzón, J.; Flórez-Elvira, L.J.; Correa, A.; Londoño, P.A.; Londoño-Mosquera, J.D.; Aragón-Muriel, A.; Polo-Cerón, D.; Ocampo-Ibáñez, I.D. Antibacterial Activity of a Cationic Antimicrobial Peptide against Multidrug-Resistant Gram-Negative Clinical Isolates and Their Potential Molecular Targets. *Molecules* **2020**, *25*, 5035. [[CrossRef](#)] [[PubMed](#)]
7. Futaki, S.; Suzuki, T.; Ohashi, W.; Yagami, T.; Tanaka, S.; Ueda, K.; Sugiura, Y. Arginine-Rich Peptides. *J. Biol. Chem.* **2001**, *276*, 5836–5840. [[CrossRef](#)] [[PubMed](#)]
8. Lengacher, R.; Marlin, A.; Śmiłowicz, D.; Boros, E. Medicinal Inorganic Chemistry—Challenges, Opportunities and Guidelines to Develop the next Generation of Radioactive, Photoactivated and Active Site Inhibiting Metal-Based Medicines. *Chem. Soc. Rev.* **2022**, *51*, 7715–7731. [[CrossRef](#)] [[PubMed](#)]
9. Abd-El-Aziz, A.S.; Agatemor, C.; Etkin, N. Antimicrobial Resistance Challenged with Metal-Based Antimicrobial Macromolecules. *Biomaterials* **2017**, *118*, 27–50. [[CrossRef](#)]
10. Łodyga-Chruścińska, E. Tetrazole Peptides as Copper(II) Ion Chelators. *Coord. Chem. Rev.* **2011**, *255*, 1824–1833. [[CrossRef](#)]
11. D’Accolti, M.; Bellotti, D.; Dzień, E.; Leonetti, C.; Leveraro, S.; Albanese, V.; Marzola, E.; Guerrini, R.; Caselli, E.; Rowińska-Żyrek, M.; et al. Impact of C- and N-terminal protection on the stability, metal chelation and antimicrobial properties of calcitermin. *Sci. Rep.* **2023**, *13*, 18228. [[CrossRef](#)] [[PubMed](#)]
12. Berdis, A.J. Inhibiting DNA Polymerases as a Therapeutic Intervention against Cancer. *Front. Mol. Biosci.* **2017**, *4*, 78. [[CrossRef](#)]
13. Long, E.C.; Fang, Y.-Y.; Lewis, M.A. DNA Minor Groove Recognition by Ni(II)- and Cu(II)-Gly-Gly-His Derived Metallopeptides. In *ACS Symposium Series*; Oxford University Press: Oxford, UK, 2009; pp. 219–241. [[CrossRef](#)]
14. O’Shaughnessy, M.; Hurley, J.; Dillon, S.C.; Herra, C.; McCarron, P.; McCann, M.; Devereux, M.; Howe, O. Antibacterial Activity of Metal-Phenanthroline Complexes against Multidrug-Resistant Irish Clinical Isolates: A Whole Genome Sequencing Approach. *J. Biol. Inorg. Chem.* **2022**, *28*, 153–171. [[CrossRef](#)] [[PubMed](#)]
15. Oñate-Garzón, J.; Manrique-Moreno, M.; Trier, S.; Leidy, C.; Torres, R.; Patiño, E. Antimicrobial activity and interactions of cationic peptides derived from *Galleria mellonella* cecropin D-like peptide with model membranes. *J. Antibiot.* **2017**, *70*, 238–245. [[CrossRef](#)]
16. Bolin, D.R.; Sytwu, I.; Humiec, F.; Meienhfer, J. Preparation of Oligomer-free N α -Fmoc and N α -urethane Amino Acids. *Int. J. Pept. Protein Res.* **1989**, *33*, 353–359. [[CrossRef](#)]
17. *Novabiochem*[®] Letters 2/06; Merck Millipore: Burlington, MA, USA, 2006; pp. 1–4.
18. Torres-García, C.; Pulido, D.; Carceller, M.; Ramos, I.; Royo, M.; Nicolás, E. Solid-Phase Synthesis of Phenylalanine Containing Peptides Using a Traceless Triazene Linker. *J. Org. Chem.* **2012**, *77*, 9852–9858. [[CrossRef](#)] [[PubMed](#)]
19. Caballero, A.B.; Terol-Ordaz, L.; Espargaró, A.; Vázquez, G.; Nicolás, E.; Sabaté, R.; Gamez, P. Histidine-Rich Oligopeptides To Lessen Copper-Mediated Amyloid- β Toxicity. *Chem. A Eur. J.* **2016**, *22*, 7268–7280. [[CrossRef](#)] [[PubMed](#)]
20. Kaiser, E.; Colecott, R.L.; Bossinger, C.D.; Cook, P.I. Color Test for Detection of Free Terminal Amino Groups in the Solid-Phase Synthesis of Peptides. *Anal. Biochem.* **1970**, *34*, 595–598. [[CrossRef](#)]
21. He, Y.; Zheng, Q.; Huang, H.; Ji, Y.; Lin, Z. Synergistic Synthesis of Hydrophilic Hollow Zirconium Organic Frameworks for Simultaneous Recognition and Capture of Phosphorylated and Glycosylated Peptides. *Anal. Chim. Acta* **2022**, *1198*, 339552. [[CrossRef](#)]
22. Clinical and Laboratory Standards Institute. *Methods for Dilution Antimicrobial Susceptibility Test for Bacteria That Grow Aerobically, Approved Standard*, 9th ed.; CLSI: Wayne, PA, USA, 2012.
23. Gajic, I.; Kabic, J.; Kekic, D.; Jovicevic, M.; Milenkovic, M.; Mitic Culafic, D.; Trudic, A.; Ranin, L.; Opavski, N. Antimicrobial Susceptibility Testing: A Comprehensive Review of Currently Used Methods. *Antibiotics* **2022**, *11*, 427. [[CrossRef](#)]
24. Polo-Cerón, D. Cu(II) and Ni(II) Complexes with New Tridentate NNS Thiosemicarbazones: Synthesis, Characterisation, DNA Interaction, and Antibacterial Activity. *Bioinorg. Chem. Appl.* **2019**, *2019*, 3520837. [[CrossRef](#)] [[PubMed](#)]
25. Rivera Franco, N.; Braga, Y.; Espitia Fajardo, M.; Barreto, G. Identifying New Lineages in the Y Chromosome of Colombian Amazon Indigenous Populations. *Am. J. Phys. Anthropol.* **2020**, *172*, 165–175. [[CrossRef](#)] [[PubMed](#)]
26. Daina, A.; Michielin, O.; Zoete, V. SwissADME: A Free Web Tool to Evaluate Pharmacokinetics, Drug-Likeness and Medicinal Chemistry Friendliness of Small Molecules. *Sci. Rep.* **2017**, *7*, 42717. [[CrossRef](#)] [[PubMed](#)]
27. Rappe, A.K.; Casewit, C.J.; Colwell, K.S.; Goddard, W.A.; Skiff, W.M. UFF, a Full Periodic Table Force Field for Molecular Mechanics and Molecular Dynamics Simulations. *J. Am. Chem. Soc.* **1992**, *114*, 10024–10035. [[CrossRef](#)]
28. Trott, O.; Olson, A.J. AutoDock Vina: Improving the Speed and Accuracy of Docking with a New Scoring Function, Efficient Optimization, and Multithreading. *J. Comput. Chem.* **2009**, *31*, 455–461. [[CrossRef](#)]

29. Gasteiger, J.; Marsili, M. A New Model for Calculating Atomic Charges in Molecules. *Tetrahedron Lett.* **1978**, *19*, 3181–3184. [[CrossRef](#)]
30. Jo, S.; Kim, T.; Iyer, V.G.; Im, W. CHARMM-GUI: A Web-based Graphical User Interface for CHARMM. *J. Comput. Chem.* **2008**, *29*, 1859–1865. [[CrossRef](#)] [[PubMed](#)]
31. Huang, J.; MacKerell, A.D. CHARMM36 All-Atom Additive Protein Force Field: Validation Based on Comparison to NMR Data. *J. Comput. Chem.* **2013**, *34*, 2135–2145. [[CrossRef](#)] [[PubMed](#)]
32. Yao, G.; Huang, Q. Theoretical and Experimental Study of the Infrared and Raman Spectra of L-Lysine Acetylation. *Spectrochim. Acta Part A Mol. Biomol. Spectrosc.* **2022**, *278*, 121371. [[CrossRef](#)]
33. Seshadri, S.; Khurana, R.; Fink, A.L. [36] Fourier Transform Infrared Spectroscopy in Analysis of Protein Deposits. In *Methods in Enzymology*; Academic Press: Cambridge, MA, USA, 1999; pp. 559–576. [[CrossRef](#)]
34. Kose, A.; Erkan, S.; Tümer, M. A Series of Phenanthroline-Imine Compounds: Computational, OLED Properties and Fluorimetric Sensing of Nitroaromatic Compounds. *Spectrochim. Acta A Mol. Biomol. Spectrosc.* **2023**, *286*, 122006. [[CrossRef](#)]
35. Fulmer, G.R.; Miller, A.J.M.; Sherden, N.H.; Gottlieb, H.E.; Nudelman, A.; Stoltz, B.M.; Bercaw, J.E.; Goldberg, K.I. NMR Chemical Shifts of Trace Impurities: Common Laboratory Solvents, Organics, and Gases in Deuterated Solvents Relevant to the Organometallic Chemist. *Organometallics* **2010**, *29*, 2176–2179. [[CrossRef](#)]
36. Fan, K.; Hsu, C.; Chen, Y. Mass Spectrometry in the Discovery of Peptides Involved in Intercellular Communication: From Targeted to Untargeted Peptidomics Approaches. *Mass Spectrom. Rev.* **2022**, *42*, 2404–2425. [[CrossRef](#)] [[PubMed](#)]
37. Shi, J.; Chen, C.; Wang, D.; Wang, Z.; Liu, Y. The Antimicrobial Peptide LI14 Combats Multidrug-Resistant Bacterial Infections. *Commun. Biol.* **2022**, *5*, 926. [[CrossRef](#)] [[PubMed](#)]
38. Rodríguez, C.A.; Vesga, O. Staphylococcus Aureus Resistente a Vancomicina. *Biomédica* **2005**, *25*, 575. [[CrossRef](#)]
39. Turnbull, P.C.B.; Sirianni, N.M.; LeBron, C.I.; Samaan, M.N.; Sutton, F.N.; Reyes, A.E.; Peruski, L.F. MICs of Selected Antibiotics for *Bacillus anthracis*, *Bacillus cereus*, *Bacillus thuringiensis*, and *Bacillus mycoides* from a Range of Clinical and Environmental Sources as Determined by the Ettest. *J. Clin. Microbiol.* **2004**, *42*, 3626–3634. [[CrossRef](#)] [[PubMed](#)]
40. Bencini, A.; Lippolis, V. 1,10-Phenanthroline: A Versatile Building Block for the Construction of Ligands for Various Purposes. *Coord. Chem. Rev.* **2010**, *254*, 2096–2180. [[CrossRef](#)]
41. Norouzi, P.; Mirmohammadi, M.; Houshdar Tehrani, M.H. Anticancer Peptides Mechanisms, Simple and Complex. *Chem. Biol. Interact.* **2022**, *368*, 110194. [[CrossRef](#)] [[PubMed](#)]
42. Yasir, M.; Dutta, D.; Willcox, M.D.P. Enhancement of Antibiofilm Activity of Ciprofloxacin against Staphylococcus Aureus by Administration of Antimicrobial Peptides. *Antibiotics* **2021**, *10*, 1159. [[CrossRef](#)] [[PubMed](#)]
43. Choosakoonkriang, S.; Lobo, B.A.; Koe, G.S.; Koe, J.G.; Middaugh, C. Russell. Biophysical Characterization of PEI/DNA Complexes. *J. Pharm. Sci.* **2003**, *92*, 1710–1722. [[CrossRef](#)]
44. Yang, S.; Zhou, X.; Li, R.; Fu, X.; Sun, P. Optimized PEI-based Transfection Method for Transient Transfection and Lentiviral Production. *Curr. Protoc. Chem. Biol.* **2017**, *9*, 147–157. [[CrossRef](#)]
45. Hellman, L.M.; Fried, M.G. Electrophoretic Mobility Shift Assay (EMSA) for Detecting Protein–Nucleic Acid Interactions. *Nat. Protoc.* **2007**, *2*, 1849–1861. [[CrossRef](#)] [[PubMed](#)]
46. Davies, A.M. A Ca²⁺-Induced Mitochondrial Permeability Transition Causes Complete Release of Rat Liver Endonuclease G Activity from Its Exclusive Location within the Mitochondrial Intermembrane Space. Identification of a Novel Endo-Exonuclease Activity Residing within the Mitochondrial Matrix. *Nucleic Acids Res.* **2003**, *31*, 1364–1373. [[CrossRef](#)] [[PubMed](#)]
47. McKie, S.J.; Desai, P.R.; Seol, Y.; Allen, A.M.; Maxwell, A.; Neuman, K.C. Topoisomerase VI Is a Chirally-Selective, Preferential DNA Decatenase. *eLife* **2022**, *11*, e67021. [[CrossRef](#)] [[PubMed](#)]
48. Meloni, B.P.; Mastaglia, F.L.; Knuckey, N.W. Cationic Arginine-Rich Peptides (CARPs): A Novel Class of Neuroprotective Agents With a Multimodal Mechanism of Action. *Front. Neurol.* **2020**, *11*, 108. [[CrossRef](#)] [[PubMed](#)]
49. Anastassopoulou, J. Metal–DNA Interactions. *J. Mol. Struct.* **2003**, *651–653*, 19–26. [[CrossRef](#)]
50. Lane, D.; Prentki, P.; Chandler, M. Use of Gel Retardation to Analyze Protein–Nucleic Acid Interactions. *Microbiol. Rev.* **1992**, *56*, 509–528. [[CrossRef](#)] [[PubMed](#)]
51. Artika, I.M.; Dewi, Y.P.; Nainggolan, I.M.; Siregar, J.E.; Antonjaya, U. Real-Time Polymerase Chain Reaction: Current Techniques, Applications, and Role in COVID-19 Diagnosis. *Genes* **2022**, *13*, 2387. [[CrossRef](#)] [[PubMed](#)]
52. Sidstedt, M.; Rådström, P.; Hedman, J. PCR inhibition in qPCR, dPCR and MPS—mechanisms and solutions. *Anal. Bioanal. Chem.* **2020**, *412*, 2009–2023. [[CrossRef](#)]
53. Agarwal, P.; Huckle, J.; Newman, J.; Reid, D.L. Trends in Small Molecule Drug Properties: A Developability Molecule Assessment Perspective. *Drug Discov. Today* **2022**, *27*, 103366. [[CrossRef](#)]

Disclaimer/Publisher’s Note: The statements, opinions and data contained in all publications are solely those of the individual author(s) and contributor(s) and not of MDPI and/or the editor(s). MDPI and/or the editor(s) disclaim responsibility for any injury to people or property resulting from any ideas, methods, instructions or products referred to in the content.